Pluripotent Stem Cell-derived Cerebral Organoids Reveal Human Oligodendrogenesis with Dorsal and Ventral Origins

Hyosung Kim[1], Ranjie Xu[1], Padmashri Ragunathan[2], Anna Dunaevsky[2], Ying Liu[3,4], Cheryl F. Dreyfus[5], Peng Jiang[1,*]

[1]Department of Cell Biology and Neuroscience, Rutgers University, Piscataway, NJ 08854, USA
[2]Department of Developmental Neuroscience, Munroe-Meyer Institute, University of Nebraska Medical Center, Omaha, NE 68198, USA
[3]Department of Neurosurgery, University of Texas Health Science Center at Houston, Houston, TX 77030, USA.
[4]Center for Stem Cell and Regenerative Medicine, the Brown Foundation Institute of Molecular Medicine for the Prevention of Human Diseases, University of Texas Health Science Center at Houston, Houston, TX 77030, USA.
[5]Department of Neuroscience and Cell Biology, Rutgers Robert Wood Johnson Medical School, Piscataway, NJ 08854, USA

*Address correspondence to:
Peng Jiang, Ph.D.
Assistant Professor
Department of Cell Biology and Neuroscience
Rutgers University
604 Allison Road, Piscataway, NJ 08854
Email: peng.jiang@rutgers.edu
Phone: 848-445-2805

Abstract

Oligodendrocytes, myelin-forming glia in the central nervous system (CNS), are the last major type of neural cells formed during the CNS development. Although the process of oligodendrogenesis has been relatively well delineated in the rodent brain at embryonic and early postnatal stages, it remains largely unknown whether analogous developmental processes are manifested in the human brain. Here, we report oligodendrogliogenesis in brain region-specific forebrain organoids, generated by using OLIG2-GFP knockin human pluripotent stem cell (hPSC) reporter lines. We found that OLIG2/GFP exhibited distinct temporal expression patterns in ventral forebrain organoids (VFOs) vs. dorsal forebrain organoids (DFOs). Two-photon calcium imaging demonstrated functional neurons and astrocytes in the DFOs. A small subset of cells in early stage DFOs expressed OLIG2 and subsequently gave rise to glutamatergic neurons. Interestingly, oligodendrogenesis could be induced in both VFOs and DFOs after neuronal maturation promoted by the newly-designed BrainPhys medium. More importantly, rebuilding neural network by fusing VFOs with DFOs to generate fused forebrain organoids (FFOs) could promote the maturation of the oligodendroglial cells. Furthermore, dorsally-derived oligodendroglial cells were able to outcompete ventrally-derived oligodendroglia and constituted the majority of the mature oligodendrocytes in FFOs after long-term culture. Thus, our organoid models that recapitulate the oligodendrogenesis with ventral and dorsal origins will serve to study the phenotypic and functional differences between human ventrally- and dorsally-derived oligodendroglia and to reveal disease mechanisms of neurodevelopmental disorders associated with cortical myelin defects.

Introduction

Oligodendrocytes are the myelinating cells in the central nervous system (CNS) and are the last major type of neural cells formed during the CNS development (Goldman and Kuypers, 2015; Zhong et al., 2018). While myelination is most notable in the white matter, myelinating oligodendrocytes are also present in the grey matter, such as cerebral cortex. Much of our current knowledge on oligodendrocyte development is obtained from studies in rodents. In the mouse forebrain, there are three distinct and sequential waves of oligodendrocyte production (Kessaris et al., 2006; Nery et al., 2001; Orentas et al., 1999). Starting at embryonic day (E) 12.5, the first wave arises from Nkx2.1-expressing precursors in the medial ganglionic eminence (Tekki-Kessaris et al., 2001), a brain structure located in the ventral embryonic telencephalon. These oligodendrocyte progenitor cells (OPCs) migrate tangentially to distant locations and colonize the entire forebrain (Kessaris et al., 2006; Klambt, 2009). Subsequently, at E15.5, a second wave emerges from precursors in the lateral and medial ganglionic eminences (Chapman et al., 2013). These OPCs also migrate to the cortex, dispersing throughout the forebrain (Kessaris et al., 2006; Klambt, 2009). These ventrally-derived first and second waves of OPCs either remain as OPCs or differentiate into myelinating oligodendrocytes in the maturing neocortex (Kessaris et al., 2006; Tripathi et al., 2011). As the developmental timeline approaches to birth, a third wave arises dorsally from precursors expressing the homeobox gene Emx1 in the cortex (Kessaris et al., 2006; Winkler et al., 2018). Interestingly, these dorsally-derived OPCs migrate locally to populate the cortex and displace the early migrating OPCs from the first two waves that initially colonize the cortical mantle (Kessaris et al., 2006; Winkler et al., 2018). Although the process of oligodendrogenesis has been well delineated in the mouse brain at embryonic and early postnatal stages, it remains largely unknown whether analogous developmental processes are manifested in the human brain, particularly the dorsally-derived third wave of oligodendrogenesis (Jakovcevski et al., 2009; Rakic and Zecevic, 2003).

Previous studies have shown that human oligodendrocyte maturation and myelination differs from that of rodent. In comparison to the rodent brain, myelination starts prenatally in the human brain (Jakovcevski and Zecevic, 2005b; Tosic et al., 2002). Human oligodendrocyte differentiation and myelination is a particularly protracted process in humans, continuing until the third decade of life (Benes et al., 1994; Miller et al., 2012). The lack of availability of functional human brain tissue prevents a detailed understanding of human oligodendrogenesis. Neural specification of human pluripotent stem cell (hPSC), including human embryonic stem cells (hESCs) and human induced pluripotent stem cells (hiPSCs), offers unprecedented opportunities for studying human neural development (Avior et al., 2016; Marchetto et al., 2011). Over the past two decades, development of differentiation protocols has generated a variety of functional neural cell types from hPSCs that are maintained in two-dimensional (2D) monolayer culture conditions (Tao and Zhang, 2016). While oligodendroglial cells have been efficiently derived from hPSC in the 2D culture system (Douvaras and Fossati, 2015; Hu et al., 2009; Liu et al., 2011; Nistor et al., 2005; Piao et al., 2015; Stacpoole et al., 2013; Wang et al., 2013), these oligodendroglial cells are mainly derived from ventral CNS regions by using ventralizing morphogens, such as sonic hedgehog (SHH) (Goldman and Kuypers, 2015). Despite this previous progress, the different developmental origins of human oligodendrogenesis have not been able to be recapitulated in 2D cultures, likely due to the lack of cell-cell/cell-matrix interactions in these monolayer cultures.

The recent development of 3-dimensional (3D) cerebral organoids derived from hPSCs offers a promising approach to understanding human brain development (Pasca, 2018), complementing 2D cell culture models. Recent studies (Lancaster et al., 2013; Mariani et al., 2015; Pasca et al., 2015; Qian et al., 2016) have shown that culturing hPSC-derived NPCs in a 3D free-floating manner generates human cerebral organoids, possessing distinct rosette-like structures that resemble the proliferation regions of human ventricular zone and laminated cerebral cortex-like structures that recapitulate early human brain development. In this study, using OLIG2-GFP knockin hPSC reporter lines (Liu et al., 2011), we generated brain region-specific dorsal forebrain organoids (DFOs) and ventral forebrain organoids (VFOs) by inhibiting or activating SHH signaling pathway, respectively. We further monitored

the temporal expression of OLIG2/GFP and examined the oligodendrogenesis in these brain region-specific organoids. Moreover, by assembling DFOs and VFOs to form fused forebrain organoids (FFOs), we found that the human oligodendroglial differentiation and maturation were significantly promoted.

Results

Distinct expression patterns of OLIG2 in hPSC-derived ventral and dorsal forebrain organoids

To examine the expression of OLIG2 in brain region-specific organoids, we generated human ventral forebrain organoids (VFOs) and dorsal forebrain organoids (DFOs) using OLIG2-GFP hPSC (hESC and hiPSC) reporter lines generated in our previous studies (Liu et al., 2011; Xue et al., 2009). To generate the brain region-specific forebrain organoids (Fig. 1A and B), we used primitive neural progenitor cells (pNPCs) that were $PAX6^+$ as the starting population (Chen et al., 2016), because utilization of these neural fate-restricted progenitors has the advantage of efficient differentiation into desired brain regions (Monzel et al., 2017). Using methods established in recent studies (Bagley et al., 2017; Birey et al., 2017; Xiang et al., 2017), VFOs were generated by activating the SHH signaling pathway using SHH and purmorphamine (Pur), a small-molecule agonist of smoothened receptor, while DFOs were generated by inhibiting SHH signaling pathway using cyclopamine A (CycA), a smoothened receptor inhibitor, from week 3 to 5. After one additional week of culturing with neural differentiation (ND) medium or OPC differentiation medium (week 6), both OLIG2-GFP hPSC-derived DFOs and VFOs exhibited subventricular/ventricular zone(sVZ)-like regions containing $SOX2^+$ neural progenitor cells (NPCs) and $\beta IIIT^+$ immature neurons (Fig. 1C). As shown in Fig. 1D and E, at week 5, both VFOs and DFOs were composed of a comparable population of Nestin-positive NPCs (93.3 ± 0.6% and 96.8 ± 0.3 for VFOs and DFOs, respectively; n = 4) and FOXG1-positive forebrain cells (94.1 ± 1.1% and 94.2 ± 0.9%, for VFOs and DFOs, respectively; n = 4). The vast majority of the cells in DFOs remained to express PAX6, which is also a marker for the NPCs in dorsal brain (92.3 ± 2.4 %, n = 4), whereas the vast majority of the cells in VFOs expressed NKX2.1, a marker of ventral prosencephalic progenitors (97.1 ± 0.2, n = 4). By using qRT-PCR, we further examined the expression of markers for dorsal forebrain, including *EMX1* and *TBR2*, and markers for ventral forebrain, including *NKX2.2*, *DLX1*, and *LHX6* in both DFOs and VFOs. EMX1 and TBR2 are expressed by cortical neural progenitors and intermediate progenitors (Englund et al., 2005; Gorski et al., 2002). NKX2.2, LHX6, and DLX1 are expressed by the neural progenitors in the medial ganglionic eminence (Briscoe et al., 1999; Du et al., 2008; Petryniak et al., 2007). As shown in Fig. 1F, we found that markers for ventral forebrain, *NKX2.2*, *DLX1*, and *LHX6,* were conspicuously detected in VFOs, whereas markers for dorsal forebrain, *EMX1* and *TBR2*, were restricted to DFOs. Although DFOs and VFOs were generated from the same population of $PAX6^+$ pNPCs at week 3 (Fig. 1B), as opposed to week 5 DFOs, nearly all the cells in week 5 VFOs were $NKX2.1^+/PAX6^-$ and abundantly expressed *NKX2.2*, *DLX1*, and *LHX6*, indicating that VFOs undergo ventral forebrain development induced by the activation of the SHH signaling pathway. Together with the data showing the restricted expression of *EMX1* and *TBR2* in DFOs, the observation that week 5 DFOs were highly enriched of $PAX6^+/NKX2.1^-$ NPCs indicates the formation of dorsal forebrain regional identity in DFOs. From week 5 to 7, intense GFP signals were observed in VFOs, whereas a small subset of cells in DFOs was found to express GFP (Fig. 1B and G). After long-term culture, robust GFP fluorescence in the VFOs became dimmer at week 9 and eventually was found to distribute evenly in the VFOs at week 12. The weak GFP signals in the DFOs gradually decreased and became undetectable at week 9. Interestingly, we observed the reappearance of GFP signals at week 12 (Fig. 1G). Furthermore, we performed qRT-PCR to examine the expression of *OLIG2* in DFOs at different time points. We consistently found that *OLIG2* expression was very low at week 5 and hardly detectable at week 9. At week 12, the *OLIG2* expression significantly increased about 25 fold, compared to its level at week 5 (Fig. 1H).

OLIG2 is cytoplasmically expressed in $PAX6^+$ neural progenitors in week 5 DFOs

GFP fluorescence faithfully mirrored the expression of OLIG2 in both VFOs and DFOs (Fig. 2A and B), consistent with our previous studies (Jiang et al., 2013; Liu et al., 2011). There was a significantly higher abundance of $OLIG2^+$ cells in VFOs (57.0 ± 7.2 %) than in DFOs (8.2 ± 0.7 %, n = 4). Notably, unlike the nuclear localization of OLIG2 in VFOs, GFP-positive cells in DFOs exhibited cytoplasmic OLIG2 expression (Fig. 2A and C). This observation was further confirmed by immunoblot analysis.

OLIG2 was abundantly present in the nuclear fraction prepared from VFOs, whereas OLIG2 was detected at a low level only in the cytoplasmic fraction prepared from DFOs (Fig. 2D). In the VFOs, nearly all GFP^+ cells expressed NKX2.1 (Fig. 2E). As predicted by virtually no detectable $NKX2.1^+$ cells in the DFOs (Fig. 1D and E), a subpopulation of GFP^+ cells in the DFOs was colocalized with PAX6 staining (31.0 ± 1.6 % of total GFP^+ cells, n = 4), further indicating the dorsal forebrain regional identity of the $OLIG2^+$ cells in the DFOs (Fig. 2E and F). Taken together, OLIG2 is not only expressed in the VFOs but also cytoplasmically expressed in a small subset of NPCs in the DFOs. Our DFOs may recapitulate a distinct but small number of OLIG2-expressing NPCs that distribute in the dorsal region of the forebrain seen in both mouse and human embryonic brain (Jakovcevski and Zecevic, 2005a; Ono et al., 2008).

$OLIG2^+$ NPCs with dorsal forebrain regional identity can give rise to glutamatergic neurons

To further examine whether NPCs in the DFOs could differentiate into functional neurons and glial cells, we performed two-photon Ca^{2+} imaging on the organoids at week 6. We recorded patterns of Ca^{2+} transients from soma of total 78 spontaneously active cells collected from randomly selected 5 fields in 2 organoids. The Ca^{2+} transients exhibited by astrocyte are slower transients whereas the ones displayed by neurons are faster transients (Ohara et al., 2009; Tashiro et al., 2002). As shown in Fig. 3A and B, based on the duration and the number of oscillations, the patterns of Ca^{2+} transients could be grouped into two types: type 1 “glia-like” cells that had a lower number of oscillations with longer durations (> 10 s) and type 2 “neuron-like” cells that had a higher number of oscillations with shorter durations (< 2 s). Type 2 “neuron-like” cells also exhibited a significantly higher peak value of Ca^{2+} transients than type 1 “glia-like” cells (Fig. 3B).

The nuclear vs. cytoplasmic localization of Olig2 in NPCs is likely an indication of fate commitment of the cells. Nuclear localization of Olig2 suggests differentiation to oligodendroglial lineage cells (Ligon et al., 2006), whereas cytoplasmic localization suggests differentiation to neuronal or astroglial cells (Setoguchi and Kondo, 2004; Takebayashi et al., 2000; Zhao et al., 2009). To delineate the cell identities, particularly the identity of GFP^+ cells, we immuno-stained the organoids with astroglial marker S100β or neuronal marker βIIIT. As shown in Fig. 3C, a large number of $βIIIT^+$ neurons and a small population of $S100β^+$ astrocytes were identified in 6-week-old DFOs. The GFP^+ NPCs in DFOs mainly differentiated into neurons with a small percent giving rise to astroglia (Fig. 3D; 3.1 ± 0.2 and 28.7 ± 4.5 % of GFP^+ cells expressed S100β and βIIIT, respectively; n = 3). $PDGFRα^+$ OPCs, however, were not detected (data not shown) in week 6 DFOs. In addition, we double-stained the DFOs with GFP and DCX, a marker for migrating immature neurons (Gleeson et al., 1999), or TBR2, a marker for intermediate neuronal progenitors (Sessa et al., 2010). We found that there were GFP^+/DCX^+ processes and that some GFP^+ cells were positive for TBR2 (Fig. 3E), further suggesting that these $GFP^+/OLIG2^+$ cells were able to differentiate to neuronal cells.

A previous fate-mapping study in mice has clearly demonstrated that a fraction of Olig2-expressing NPCs in the telecephalon and diencephalon in the fetal forebrain develop into glutamatergic neurons (Ono et al., 2008). We found the formation of glutamatergic synapses in week 7 DFOs, as indicated by the staining of $VGLUT1^+$ puncta (Fig. 3G). Notably, some of the $VGLUT1^+$ puncta were found to distribute along the GFP^+ processes. This prompted us to further characterize whether the $OLIG2^+$ cells in the DFOs could also give rise to glutamatergic neurons. We triple-stained the week 7 DFOs with GFP, βIIIT, and glutaminase (GLS) that is the enzyme essential for glutamate production and is expressed by glutamatergic neurons and astrocytes in the brain (Aoki et al., 1991; Cardona et al., 2015). We found that a small population of GFP^+ neurons, marked by βIIIT, expressed GLS (Fig. 3F), suggesting that the $OLIG2^+/GFP^+$ cells in the DFOs develop into glutamatergic neurons.

BrainPhys medium promotes neuronal maturation in both VFOs and DFOs

During embryonic brain development, neurogenesis precedes gliogenesis. Oligodendroglia is the last type of glial cells formed during brain development. In addition, mounting evidence suggests that neuronal maturation and activity influence oligodendrogenesis and myelination (Gibson et al., 2014;

Mitew et al., 2018). A recent study developed a new BrainPhys medium with adjusted concentrations of inorganic salts, neuroactive amino acids, and energetic substrates to better support the neurophysiological activity of cultured human neurons (Bardy et al., 2015). We further cultured DFOs and VFOs in the BrainPhys medium from week 7 to 9 (Fig. 4A). Then we examined the expression of c-Fos, an activity-dependent immediate early gene that is expressed in neurons following depolarization and often used as a marker for mapping neuronal activity (Loebrich and Nedivi, 2009). After culture in BrainPhys medium, neuronal maturation and activity were significantly promoted in both DFOs and VFOs, compared to the organoids cultured in the commonly used ND medium. As shown in Fig. 4A and B, at week 9, there were significantly more c-Fos$^+$ cells in the organoids cultured in BrainPhys medium than in ND medium. Furthermore, we observed that the synaptic markers, postsynaptic density protein 95 (PSD-95) and synapsin 1 were also expressed in the DFOs cultured in BrainPhys medium (Fig. 4C). Moreover, neurons expressing CUX1, a marker for superficial-layer cortical neurons (Nieto et al., 2004) and neurons expressing TBR1$^+$, a marker for pre-plate/deep-layer neurons (Hevner et al., 2001) were also seen in the DFOs (Fig. 4D). A small population of Emx1$^+$ dorsal NPCs was also found in DFOs (6.45 ± 0.9%, n = 4; Fig. 4E and F). At this time point, GFP signals became undetectable in the DFOs. In the VFOs, GFP fluorescence became much dimmer, compared to week 7 VFOs (Fig. 1G). This may result from the differentiation of a subset of OLIG2-expressing ventral forebrain NPCs to neurons, particularly interneurons, and subsequent termination of OLIG2/GFP expression in those cells, as reported in previous studies in mice (Miyoshi et al., 2007; Ono et al., 2008).

Human PSC-derived organoids reveal the ventral and dorsal origins of oligodendrogenesis

To promote oligodendrogenesis in the DFOs and VFOs, we further cultured the organoids for an additional 3 weeks (Fig. 4A; week 9 to 12) in oligodendroglial differentiation medium containing thyroid hormone T3, which is commonly used to promote oligodendroglial differentiation from hPSCs under 2D culture conditions (Douvaras and Fossati, 2015; Hu et al., 2009; Liu et al., 2011; Nistor et al., 2005; Piao et al., 2015; Stacpoole et al., 2013; Wang et al., 2013). As shown in Fig. 1G, at week 12, there were a large number of bright GFP$^+$ cells evenly distributed in the VFOs. In the DFOs, GFP signal reappeared after the treatment of T3. To characterize the identity of these GFP$^+$ cells, we double-stained GFP with OPC marker PDGFRα. We found that in both VFOs and DFOs, nearly half of the GFP$^+$ expressed PDGFRα, indicating the oligodendrogenesis in both organoids (Fig. 4G and H). A subset of PDGFRα$^+$ OPCs in DFOs also exhibited immunoreactivity for Ki67, suggesting that these OPCs were capable of proliferation (Fig. 4I). In addition, we also stained the organoids with S100β or βIIIT, but found no GFP$^+$ cells expressing S100β or βIIIT at week 12 (data not shown). Thus, the GFP$^+$/PDGFRα-negative cells in the organoids might have committed to oligodendroglial fate but had not yet expressed any OPC marker. To further validate the ventral vs. dorsal origin of the OPCs in VFOs and DFOs, we examined the expression of tyrosine kinase B (TrkB). Previous studies (Du et al., 2003) have shown that TrkB is selectively expressed in oligodendroglia from the basal forebrain that has a ventral origin (Kessaris et al., 2006; Klambt, 2009), but not expressed in oligodendroglia from cerebral cortex that has a dorsal origin (Kessaris et al., 2006; Winkler et al., 2018). We observed that TrkB was robustly expressed by neurons in both VFOs and DFOs. However, only a small population of TrkB$^+$/GFP$^+$ cells were seen in VFOs but no TrkB$^+$/GFP$^+$ cells in DFOs (Fig. 4J). These results demonstrate that further culturing VFOs and DFOs under conditions favoring oligodendroglial differentiation can further reveal oligodendrogenesis with ventral and dorsal origins, respectively.

Oligodendroglial maturation in DFOs, VFOs, and fused forebrain organoids (FFOs)

To examine whether OPCs in these organoids were able to mature into myelinating oligodendrocytes, we further cultured the VFOs and DFOs in OL medium up to 6 weeks. Moreover, to test whether the interregional interactions between the differentially patterned human forebrain organoids (Bagley et al., 2017; Birey et al., 2017; Xiang et al., 2017) are important for oligodendroglial maturation, we generated FFOs and further cultured them in OL medium (Fig. 5A). VFOs at an early stage (week 5) were used for fusion with DFOs because previous studies showed that immature migrating interneurons generated by

ventral forebrain NPCs promote oligodendrocyte formation in the cortex in a paracrine fashion (Voronova et al., 2017). After fusion, we observed a massive migration of GFP^+ cells from the VFOs into the DFOs (Fig. 5B), similar to the observations reported in previous studies (Bagley et al., 2017; Birey et al., 2017; Xiang et al., 2017). At 3 weeks after fusion (week 12), GFP^+ cells largely populated the FFOs and exhibited bipolar morphology, characteristics of OPCs (Fig. 5B). At week 15, we assessed oligodendroglial maturation in DFOs, VFOs, and FFOs by staining MBP, a marker for mature oligodendrocytes. As shown in Fig. 5C and D, MBP^+/GFP^+ cells were detected in VFOs (1.0 ± 0.4%, n = 4), but not in DFOs. Interestingly, fusing the organoids significantly promote the maturation of oligodendrocytes, as indicated by a higher percent of MBP^+/GFP^+ cells in FFOs (8.4 ± 2.0%, n = 4). The mature oligodendrocytes in FFOs exhibited complex processes at week 12 (Fig. 5E, upper panel) and occasionally, we observed tubular-shaped MBP staining in FFOs at week 15 (Fig. 5E, bottom panel), suggesting that the oligodendrocytes started to myelinate axons. To further examine whether the mature oligodendrocytes formed myelin sheath in the FFOs, we performed EM analysis. We examined myelin ultrastructure in 8 sections from 4 FFOs. In total, we identified 52 myelinated axons. As shown in Fig. 5F**,** axons with loose escheatment by a few myelin laminae and some axons with compact myelin were observed in week 15 FFOs, which is similar to the “unorganized” myelin structure observed in oligocortical spheroids in a recent study (Madhavan et al., 2018a) and also partly resembles the earliest stage of in vivo fetal myelinogenesis in humans (Weidenheim et al., 1992).

We next performed qRT-PCR to examine the expression of markers for excitatory and inhibitory neurons as well as markers for inhibitory and excitatory synapses in VFOs, DFOs, and FFOs. As shown in Fig. 5G, we found that the gene transcripts encoding markers for inhibitory neurons, including *SLC6A1* and *GAD1* that respectively encode GABA transporter type 1 and glutamate decarboxylase 1, were expressed at much higher levels in VFOs than in DFOs. In contrast, gene transcripts encoding markers for excitatory neurons, including *SLC17A7* and *SLC17A6* that respectively encode vesicular glutamate transporters VGLUT1 and VGLUT2, were expressed at higher levels in DFOs than in VFOs. Importantly, we found that FFOs exhibited well-balanced expression of all these gene transcripts, as compared to DFOs and VFOs. FFOs exhibited not only significantly enhanced expression of markers for inhibitory neurons *SLC6A1* and *GAD1*, compared to DFOs, but also enhanced expression of markers for excitatory neurons *SLC17A7* and *SLC17A6*, compared to VFOs. Furthermore, we examined the expression of gene transcripts encoding the components of post-synaptic machinery, such as *HOMER1* and *SHANK3* that respectively encode excitatory postsynaptic components HOMER and SHANK; and *ARHGEF9* and *GPHN* that respectively encode inhibitory postsynaptic components COLLYBISTIN and GEPHYRIN. Compared to DFOs and VFOs, FFOs exhibited significantly enhanced expression of the gene transcripts encoding components of both inhibitory and excitatory postsynaptic. We also observed that the expression of gene transcripts for inhibitory postsynaptic components was higher in VFOs than in DFOs, and the expression of gene transcripts for excitatory postsynaptic components was similar in VFOs and DFOs. These findings demonstrate that the FFOs generated in our study possess integrated glutamatergic and GABAergic neurons, and have enhanced expression of synaptic markers, consistent with the results reported in recent studies (Birey et al., 2017; Xiang et al., 2017). Notably, the expression of *MBP* gene transcript was also significantly higher in FFOs than in DFOs or VFOs. *PDGFRα* gene transcript was expressed at a similar level in FFOs and VFOs, but at a lower level in DFOs. Because previous studies demonstrate that neuronal network and activity promote oligodendroglial differentiation and maturation (Gibson et al., 2014; Mitew et al., 2018), our obervation suggests that enhanced neuronal network in our organoids might contribute to oligodendroglial differentiation and maturation.

Dorsally-derived oligodendroglia outcompete ventrally-derived oligodendroglia in the FFOs

To further examine which population of oligodendroglia constituted the oligodendroglial cells in FFOs, we generated a new version of fused forebrain organoids, by fusing the VFOs and DFOs that were respectively derived from isogenic OLIG2-GFP hiPSC reporter line and ND2.0 hiPSCs that do not have any reporter fluorescence (Fig. 6A). The isogenicity of OLIG2-GFP hiPSCs and ND2.0 hiPSCs were

indicated by the identical short tandem repeat (STR) genotyping profile (Supplementary Table 1). In addition, we did not observe any growth advantage on one line versus the other between the two iPSC lines. Then we examined the interactions between ventrally- and dorsally-derived oligodendroglia in those FFOs. Since OLIG2 is expressed in all oligodendroglial lineage cells (Ligon et al., 2006), in this setting, dorsally- and ventrally-derived oligodendroglia could be readily distinguished because the former would be GFP-negative/OLIG2$^+$, whereas the latter would be GFP$^+$/OLIG2$^+$. As shown in Fig. 6B and C, we observed that at one week after fusion (week 10), the ventrally-derived GFP$^+$/OLIG2$^+$ cells outnumbered the dorsally-derived GFP-negative/OLIG2$^+$ cells. At 3 and 6 weeks after fusion (week 12 and 15), the dorsally-derived GFP-negative/OLIG2$^+$ cells became a dominant population, whereas the percentage of ventrally-derived GFP$^+$/OLIG2$^+$ cells among total OLIG2$^+$ cells dramatically decreased in the FFOs from week 10 to 15 (Fig. 6B and C). Furthermore, at week 12, the majority of MBP$^+$ cells were MBP$^+$/GFP-negative (Fig. 6D and E), suggesting that those mature oligodendrocytes had a dorsal origin. Taken together, these results demonstrate that the majority of oligodendroglia in the FFO at an early stage (week 10) are ventrally-derived oligodendroglia, which are outcompeted by dorsally-derived oligodendroglia in the FFOs at later stages (week 12 and 15).

Discussion

The transcription factor Olig2 is not only closely associated with the development of oligodendrocytes in the vertebrate CNS, but also is expressed in NPCs during development (Jiang et al., 2013; Ligon et al., 2006; Meijer et al., 2012; Ono et al., 2008). It is well known that at early embryonic stages in mice, Olig2 is mostly expressed in the brain by the NPCs that distribute in the ventral telencephalon (Ligon et al., 2006; Meijer et al., 2012). A distinct but small number of Olig2-expressing NPCs that distribute in the dorsal region of the forebrain, specifically in the dorsal diencephalon, has been identified in both mouse and human embryonic brain (Jakovcevski and Zecevic, 2005a; Ono et al., 2008). We observed distinct temporal expression patterns of OLIG2 in DFOs and VFOs. This was achieved by using our OLIG2-GFP hPSC reporter lines, which allow us to monitor OLIG2 expression by real-time monitoring GFP fluorescence. In our DFO model, the small population of human $OLIG2^+/PAX6^+$ NPCs seen in the week 5 DFOs may mimic that population of $OLIG2^+$ NPCs in the human embryonic diencephalon (Jakovcevski and Zecevic, 2005a). Furthermore, we demonstrate that these early human $OLIG2^+$ NPCs are also able to give rise to glutamatergic neurons and astrocytes in the organoids, similar to the mouse $Olig2^+$ NPCs in the fetal forebrain (Ono et al., 2008).

Interestingly, we revealed oligodendrogenesis with a dorsal origin in our organoid models. This oligodendrogenesis in DFOs cultured by itself or as a part of FFOs likely recapitulates the 3rd wave of oligodendrogenesis seen in the mouse brain because: First, these oligodendroglial cells are dorsally-derived. In this study, the DFOs are generated by using pNPCs as the starting population, since these neural fate-restricted pNPCs retain high responsiveness to instructive neural patterning cues (Li et al., 2011) and can be efficiently patterned to desired brain regions (Monzel et al., 2017). In addition, we treated the organoids with CycA to further enhance dorsal forebrain identity (Bagley et al., 2017; Vazin et al., 2014). Since we did not observe any ventral forebrain NPCs in these organoids, all neural derivatives, including oligodendroglial lineage cells, generated in the DFOs have a dorsal origin. Second, these oligodendroglial cells are derived from progenitors that are distinct from the early $OLIG2^+/PAX6^+$ progenitor cells. At week 9, all $OLIG2^+/PAX6^+$ NPCs differentiate to neurons or astrocytes, and OLIG2 expression terminates as indicated by GFP fluorescence and qPCR results. Moreover, we find $Emx1^+$ dorsal forebrain neural precursors in the 9-week-old organoids. It is very likely that those $Emx1^+$ cells further differentiate to $OLIG2^+/GFP^+$ oligodendroglial cells under the culture condition favoring oligodendroglial differentiation, similar to the findings in the mouse brain (Kessaris et al., 2006; Winkler et al., 2018). Third, the newly emerged $OLIG2^+$ cells in week 12 DFOs express PDGFRα, indicating their OPC nature. Furthermore, there OPCs are able to proliferate and populate the organoids. Lastly, these dorsally-derived oligodendroglia can outcompete ventrally-derived oligodendroglia in the FFOs, which may mimic the process of oligodendrogenesis in the cerebral cortex, where the early oligodendroglia are derived from the embryonic ventral forebrain, such as medial ganglionic eminence and anterior entopeduncular area, and these early-born oligodendroglia are outcompeted by oligodendroglia with a dorsal origin at late developmental stages (Kessaris et al., 2006). Taken together, in this study, we establish new cerebral organoid models that recapitulate the dorsal $OLIG2^+$ NPCs and reveal that a dorsal origin of oligodendrogenesis may occur during human brain development.

Technically, we also develop new organoid models with significantly accelerated oligodendroglial maturation. Deriving mature oligodendrocytes from human PSCs is a tedious and lengthy process, and developing new methods to obtain human mature oligodendrocytes within a shortened timeframe has been a major research effort (Douvaras and Fossati, 2015; Goldman and Kuypers, 2015; Liu et al., 2011; Stacpoole et al., 2013). In our system, MBP^+ mature oligodendrocytes appeared at 9 weeks after organoid formation, as opposed to 20 weeks after organoid formation as reported by a recent study (Madhavan et al., 2018b) (~11 weeks quicker). This acceleration of the oligodendroglial maturation program in our organoids is likely achieved by promoting neuronal maturation with the newly-designed BrainPhys medium and rebuilding the neuronal network through fusing DFOs and VFOs. Balanced excitatory and inhibitory neuronal activities (Nagy et al., 2017), neurotransmitters and neurotrophins

released by excitatory neurons or astrocytes (Gautier et al., 2015; Lundgaard et al., 2013; Xiao et al., 2009), as well as cytokines released by young migrating inhibitory neurons (Voronova et al., 2017) may partly contribute to the enhanced oligodendrogliogenesis and oligodendroglial lineage progression in FFOs. As compared to the fusion methods, generating a single, regionalized organoids containing both ventral and dorsal elements may more precisely recapitulate the serial waves of oligodendroglial production and replacement seen in the developing forebrain, because the different germinal zones within single organoids might be well preserved and not be disrupted by the fusion process. Future improvement in using novel biomaterials to induce neural patterning by releasing morphogens in a controllable and predictable way (Pasca, 2018; Wu et al., 2017) may help generate such single organoids containing both ventral and dorsal elements. Notably, similar to the recent studies (Madhavan et al., 2018a; Marton et al., 2019), the maturation of human OPCs to oligodendrocytes is not efficient in organoids, and those myelinated axons often show wrapping with multiple layers of uncompacted myelin. This may be attributed in part to a lack of oxygen penetration in the organoids cultured for long-term, which can result in necrosis in the core of organoids (Brawner et al., 2017; Giandomenico and Lancaster, 2017). As opposed to rodent OPCs, human OPC differentiation and myelination are highly sensitive to hypoxic conditions (Gautier et al., 2015). Future studies aiming at integrating a vascular structure that brings the adequate delivery of oxygen and nutrients to organoids and promoting neuronal maturation and electrical activity (Brawner et al., 2017; Mansour et al., 2018) may help facilitate organoid models with robust oligodendroglial maturation.

Previous studies using transgenic mouse models have helped us understand the developmental differences between ventrally- and dorsally-derived OPCs (Kessaris et al., 2006; Nery et al., 2001; Orentas et al., 1999; Winkler et al., 2018). However, it is largely unclear what the phenotypic and functional differences are between the different populations of OPCs. Due to the scarcity of available functional human brain tissue, no information is available on the differences in humans. In this study, we demonstrate the generation of dorsally- and ventrally-derived human oligodendroglial cells in organoids. We propose that the competitive advantage exhibited by dorsally-derived over ventrally-derived OPCs may partly result from their unique expression pattern of molecules involved in controlling OPC proliferation and lineage progression, for example GPR17, a G-protein-coupled membrane receptor suggested as an intrinsic timer of oligodendroglial differentiation during development (Chen et al., 2009; Fumagalli et al., 2011), and transcription factor EB (TFEB), which recently has been identified to govern the regional and temporal specificity of oligodendroglial differentiation and myelination (Sun et al., 2018). Future gene expression profiling studies at a single-cell level examining oligodendroglial lineage cells in the separate dorsal and ventral forebrain organoids as well as FFOs will significantly advance our understanding of the differences between human ventrally- and dorsally-derived OPCs. Combing with human iPSC technologies, examining ventrally- and dorsally-derived oligodendroglial cells in organoids with ventral and dorsal elements may be more informative to understand disease mechanisms of neurodevelopmental disorders associated with myelin defects. These organoid models could also have important implications in the setting of CNS injury, as distinct populations of human OPCs might respond to pro-myelinating drugs differently, preferentially contributing to remyelination, thus enabling a better model for therapeutic manipulation.

EXPERIMENTAL MODEL AND SUBJECT DETAILS

Culture and derivation of hPSC cell lines

The OLIG2-GFP knockin hPSCs (hESCs and hiPSCs) were established using a gene-targeting protocol and fully characterized, as reported in our previous studies (Liu et al., 2011; Xue et al., 2016). The OLIG2-GFP hiPSC reporter line was established from the ND2.0 hiPSC line that was obtained from Center for Regenerative Medicine, National Institutes of Health. The hPSCs maintained under a feeder-free condition on a hESC-qualified Matrigel (Corning)-coated dish with mTeSR1 media (STEMCELL Technologies) were used for this study. The hPSCs were passaged approximately once per week by ReLeSR media (STEMCELL Technologies). All the hPSC studies were approved by the committees on stem cell research at Rutgers University.

METHODS DETAILS

Generation of human forebrain organoids

To avoid non-CNS differentiated tissue and reduce variability in 3D cerebral organoids generation, we used purified pNPCs as the starting population for generating organoids. As shown in Fig. 1A, we induced pNPCs from hPSCs using a small molecule-based protocol (Chen et al., 2016; Li et al., 2011). Briefly, neural differentiation was induced by dual inhibition of SMAD signaling (Chambers et al., 2009) with inhibitors SB431542 (5 μM, Stemgent) and noggin (50 ng/ml, Peprotech) for a week. The embryoid bodies (EB) were then plated on dishes coated with growth factor-reduced Matrigel (BD Biosciences) in the medium consisting of DMEM/F12, 1x N2, and laminin (1 μg/ml; Sigma-Aldrich) for a week. Next, neural rosettes were manually isolated from the expanded area. The isolated neural rosettes were further cultured in pNPC media, composed of a 1:1 mixture of Neurobasal (Thermo Fisher Scientific) and DMEM/F12, supplemented with 1 x N2, 1 x B27-RA (Thermo Fisher Scientific), FGF2 (20 ng/ml, Peprotech), human leukemia inhibitory factor (hLIF, 10 ng/ml, Millipore), CHIR99021 (3 μM, Stemgent), SB431542 (2 μM), and ROCK inhibitor Y-27632 (10 μM, Tocris). To generate organoids, dissociated pNPCs by TrypLE Express (Thermo Fisher Scientific) were placed into low-attachment 96-well plates at a density of 9,000 cells to develop uniform organoids for two days. The pNPC aggregates were then grown and patterned in low-attachment 6-well plates with the treatment of either 5 μM Cyclopamine A (Cyc A; Calbiochem) for dorsalization or dual activation of SHH pathway with sonic hedgehog (SHH; 50 ng/ml, Peprotech) and purmorphamine (Pur; 1 μM, Cayman Chem) for ventralization. Starting from week 5, the DFOs were cultured on an orbital shaker with a speed of 80 rpm/min in neuronal differentiation (ND) medium containing a 1:1 mixture of Neurobasal and DMEM/F12, supplemented with 1 x N2, 1 x B27, BDNF (20 ng/ml, Peptrotech), GDNF (20 ng/ml, Peprotech), dibutyryl-cyclic AMP (1mM, Sigma), and ascorbic acid (200 nM, Sigma). The 5-week-old VFOs were cultured in oligodendrocyte progenitor cell (OPC) medium containing DMEM/F12, supplemented with 1 x N2, 1 x B27, FGF2 (10 ng/ml, Peptrotech), PDGF-AA (10 ng/ml, Peprotech). For further neuronal maturation, both DFOs and VFOs were cultured in BrainPhys medium (STEMCELL Technologies). Starting from week 9, organoids were maintained in ND medium supplemented with 3,3,5-Triiodo-L-thyronine sodium salt (T3; 10 ng/ml, Cayman Chem; OL medium) for oligodendroglial differentiation and maturation. FFOs were generated by using a spontaneous fusion method (Bagley et al., 2017; Birey et al., 2017; Xiang et al., 2017) with modifications. Briefly, single week 9 DFO were closely placed with a week 5 VFO by transferring both of them into the round-bottom ultra-low-attachment 96-well plate for 2 days without agitating. Then, the FFOs were transferred to an ultra-low-attachment 6-well plate and cultured for a day without agitating. The next day, the FFOs were maintained with OL medium on an orbital shaker with a speed of 80 rpm/min.

RNA isolation and qRT-PCR

Total RNA extracted from organoids with RNAeasy kit (Qiagen) was used to make complementary DNA with a Superscript III First-Strand kit (Invitrogen). The qRT-PCR was performed with TaqMan primers listed in supplementary table 2 on an Abi 7500 Real-Time PCR system. Experimental samples were analyzed by normalization with the expression level of housekeeping gene glyceraldehyde-3-phosphate dehydrogenase (GAPDH). Relative quantification was performed by applying the $2^{-\Delta\Delta Ct}$ method (Livak and Schmittgen, 2001).

Western blotting

OLIG2 protein expression and localization in cells were evaluated by immunoblotting using fractionated samples. The nuclear and cytoplasmic fraction was achieved by modification of a reported method (Suzuki et al., 2010). Briefly, organoids were washed with PBS and harvested. Resuspended organoids in 900 ul of ice-cold lysis buffer (0.1% NP40 in PBS) were lysed 10 times through a 25-gauge syringe. Following the second spinning down for 30 seconds, the supernatant was collected as a cytosolic fraction. 3 times washed pellet was lysed in sample buffer containing 1% of SDS. Fractionated proteins were separated on 12% SDS-PAGE gel and transferred onto nitrocellulose membrane. Blots were then blocked in 2% skim milk and incubated with primary antibodies at 4°C overnight. The information for primary antibodies and dilutions is listed in Supplementary table 3. Afterward, the blots were incubated with secondary antibodies conjugated with a fluorophore for an hour at room temperature. Western blot was visualized using Odyssey (LiCor).

Immunostaining and cell counting

Organoids fixed with 4% paraformaldehyde were processed and cryo-sectioned for immunofluorescence staining. The information for primary antibodies and dilutions is listed in Table S2. Slides were mounted with the anti-fade Fluoromount-G medium containing 1,40,6-diamidino-2-phenylindole dihydrochloride (DAPI) (Southern Biotechnology). Images were captured with LSM800 confocal microscope. The cells were counted with ImageJ software. At least six fields chosen randomly from three sections of each organoid were counted. For each organoid, at least 400 cells were counted.

Dye loading and calcium imaging

For calcium imaging in organoids, DFOs were placed on the growth factor-reduced Matrigel-coated coverslip in 6-well plate for 24 hr. The next day, organoids were loaded with fluo-4 AM (5 µM, Molecular Probes) and 0.04% Pluronic F-127 for 40 minutes and then transferred to the neuronal differentiation (ND) medium for at least 30 minutes before transferring to the submersion-type recording chamber (Warner) superfused at room temperature with artificial CSF (ACSF, mM: 126 NaCl, 3 KCl, 1.25 NaH_2PO_4, 1 $MgSO_4$, 2 $CaCl_2$, 26 $NaHCO_3$, and 10 dextrose) saturated with 95% O_2/5% CO_2. All imaging was performed with a two-photon microscope (Moving Objective Microscope; Sutter Instruments) coupled to a Ti:Sapphire laser (Chameleon Vision II, Coherent). Images were collected with a Nikon water immersion objective (25X, 1.05 NA). Excitation power measured at the back aperture of the objective was typically about 20-30 mW, and laser power was modulated using a Pockels cell. Fluo-4 was excited at 820nm and emission was detected with GaAsP detector (Hamamatsu Photonics) fitted with a 535/50 bandpass filter and separated by a 565 nm dichroic mirror. ScanImage (v5.1, Vidrio Technologies) software (Pologruto et al., 2003) was used for imaging. Time-lapse imaging was performed every 1 s for 5 minutes and was collected at 512 by 512-pixel resolution. Image analysis was performed using ImageJ software. Regions of interest (ROIs) were placed around soma. Fluorescence was averaged over ROIs placed and expressed as relative fluorescence changes ($\Delta F/F$) after subtraction of background fluorescence from a neighboring region. For each ROI, basal fluorescence was determined during 20 s periods with no Ca^{2+} fluctuation. Ca^{2+} transients were detected when fluorescence intensity reached higher than 2 SD value of baseline fluorescence intensity.

Electron microscopy

Organoid samples were fixed with 2% glutaraldehyde, 2% paraformaldehyde, and 0.1M sodium cacodylate in PBS. The selected vibratome sections were post-fixed and processed for electron microscopy (EM) as described in our previous studies (Chen et al., 2016; Jiang et al., 2016). EM images were captured using a high-resolution charge-coupled device (CCD) camera (FEI).

DNA fingerprinting short tandem repeat (STR) analysis

STR analysis was performed using GENEprint PowerPlex 16 kit (Promega performed by Cell Line Genetics. LLC). Samples were run in duplicate and blinded to the interpreter to confirm the results. Please note that ND2.0 and OLIG2-GFP hiPSC lines have identical STR genotyping profile, indicating that they are isogenic lines derived from the same parental cell line.

Statistical analysis

All experiments were repeated at least three times. Unless otherwise noted, at least 20 organoids derived from OLIG2-GFP hESCs and hiPSCs were analyzed for each experiment. Data are presented as mean ± S.E.M. and were analyzed using one-way ANOVA in combination with Tukey post-hoc test or Student's *t*-test. For statistical significance, p values < 0.05 were considered significant.

Acknowledgments

This work was in part supported by grants from the NIH (R21HD091512 and R01NS102382 to P.J.) and a pilot grant from Rutgers Brain Health Institute to P.J.

Competing Financial Interests

The authors declare no competing financial interests.

References:

Aoki, C., Kaneko, T., Starr, A., and Pickel, V.M. (1991). Identification of mitochondrial and non-mitochondrial glutaminase within select neurons and glia of rat forebrain by electron microscopic immunocytochemistry. J Neurosci Res *28*, 531-548.

Avior, Y., Sagi, I., and Benvenisty, N. (2016). Pluripotent stem cells in disease modelling and drug discovery. Nat Rev Mol Cell Biol *17*, 170-182.

Bagley, J.A., Reumann, D., Bian, S., Levi-Strauss, J., and Knoblich, J.A. (2017). Fused cerebral organoids model interactions between brain regions. Nat Methods *14*, 743-751.

Bardy, C., van den Hurk, M., Eames, T., Marchand, C., Hernandez, R.V., Kellogg, M., Gorris, M., Galet, B., Palomares, V., Brown, J., *et al.* (2015). Neuronal medium that supports basic synaptic functions and activity of human neurons in vitro. Proc Natl Acad Sci U S A *112*, E2725-2734.

Benes, F.M., Turtle, M., Khan, Y., and Farol, P. (1994). Myelination of a key relay zone in the hippocampal formation occurs in the human brain during childhood, adolescence, and adulthood. Arch Gen Psychiatry *51*, 477-484.

Birey, F., Andersen, J., Makinson, C.D., Islam, S., Wei, W., Huber, N., Fan, H.C., Metzler, K.R.C., Panagiotakos, G., Thom, N., *et al.* (2017). Assembly of functionally integrated human forebrain spheroids. Nature *545*, 54-59.

Brawner, A.T., Xu, R., Liu, D., and Jiang, P. (2017). Generating CNS organoids from human induced pluripotent stem cells for modeling neurological disorders. Int J Physiol Pathophysiol Pharmacol *9*, 101-111.

Briscoe, J., Sussel, L., Serup, P., Hartigan-O'Connor, D., Jessell, T.M., Rubenstein, J.L., and Ericson, J. (1999). Homeobox gene Nkx2.2 and specification of neuronal identity by graded Sonic hedgehog signalling. Nature *398*, 622-627.

Cardona, C., Sanchez-Mejias, E., Davila, J.C., Martin-Rufian, M., Campos-Sandoval, J.A., Vitorica, J., Alonso, F.J., Mates, J.M., Segura, J.A., Norenberg, M.D., *et al.* (2015). Expression of Gls and Gls2 glutaminase isoforms in astrocytes. Glia *63*, 365-382.

Chambers, S.M., Fasano, C.A., Papapetrou, E.P., Tomishima, M., Sadelain, M., and Studer, L. (2009). Highly efficient neural conversion of human ES and iPS cells by dual inhibition of SMAD signaling. Nat Biotechnol *27*, 275-280.

Chapman, H., Waclaw, R.R., Pei, Z., Nakafuku, M., and Campbell, K. (2013). The homeobox gene Gsx2 controls the timing of oligodendroglial fate specification in mouse lateral ganglionic eminence progenitors. Development *140*, 2289-2298.

Chen, C., Kim, W.Y., and Jiang, P. (2016). Humanized neuronal chimeric mouse brain generated by neonatally engrafted human iPSC-derived primitive neural progenitor cells. JCI Insight *1*, e88632.

Chen, Y., Wu, H., Wang, S., Koito, H., Li, J., Ye, F., Hoang, J., Escobar, S.S., Gow, A., Arnett, H.A., *et al.* (2009). The oligodendrocyte-specific G protein-coupled receptor GPR17 is a cell-intrinsic timer of myelination. Nat Neurosci *12*, 1398-1406.

Douvaras, P., and Fossati, V. (2015). Generation and isolation of oligodendrocyte progenitor cells from human pluripotent stem cells. Nat Protoc *10*, 1143-1154.

Du, T., Xu, Q., Ocbina, P.J., and Anderson, S.A. (2008). NKX2.1 specifies cortical interneuron fate by activating Lhx6. Development *135*, 1559-1567.

Du, Y., Fischer, T.Z., Lee, L.N., Lercher, L.D., and Dreyfus, C.F. (2003). Regionally specific effects of BDNF on oligodendrocytes. Dev Neurosci *25*, 116-126.

Englund, C., Fink, A., Lau, C., Pham, D., Daza, R.A., Bulfone, A., Kowalczyk, T., and Hevner, R.F. (2005). Pax6, Tbr2, and Tbr1 are expressed sequentially by radial glia, intermediate progenitor cells, and postmitotic neurons in developing neocortex. J Neurosci *25*, 247-251.

Fumagalli, M., Daniele, S., Lecca, D., Lee, P.R., Parravicini, C., Fields, R.D., Rosa, P., Antonucci, F., Verderio, C., Trincavelli, M.L., *et al.* (2011). Phenotypic changes, signaling pathway, and functional correlates of GPR17-expressing neural precursor cells during oligodendrocyte differentiation. J Biol Chem *286*, 10593-10604.

Gautier, H.O., Evans, K.A., Volbracht, K., James, R., Sitnikov, S., Lundgaard, I., James, F., Lao-Peregrin, C., Reynolds, R., Franklin, R.J., *et al.* (2015). Neuronal activity regulates remyelination via glutamate signalling to oligodendrocyte progenitors. Nat Commun *6*, 8518.

Giandomenico, S.L., and Lancaster, M.A. (2017). Probing human brain evolution and development in organoids. Curr Opin Cell Biol *44*, 36-43.

Gibson, E.M., Purger, D., Mount, C.W., Goldstein, A.K., Lin, G.L., Wood, L.S., Inema, I., Miller, S.E., Bieri, G., Zuchero, J.B., *et al.* (2014). Neuronal activity promotes oligodendrogenesis and adaptive myelination in the mammalian brain. Science *344*, 1252304.

Gleeson, J.G., Lin, P.T., Flanagan, L.A., and Walsh, C.A. (1999). Doublecortin is a microtubule-associated protein and is expressed widely by migrating neurons. Neuron *23*, 257-271.

Goldman, S.A., and Kuypers, N.J. (2015). How to make an oligodendrocyte. Development *142*, 3983-3995.

Gorski, J.A., Talley, T., Qiu, M., Puelles, L., Rubenstein, J.L., and Jones, K.R. (2002). Cortical excitatory neurons and glia, but not GABAergic neurons, are produced in the Emx1-expressing lineage. J Neurosci *22*, 6309-6314.

Hevner, R.F., Shi, L., Justice, N., Hsueh, Y., Sheng, M., Smiga, S., Bulfone, A., Goffinet, A.M., Campagnoni, A.T., and Rubenstein, J.L. (2001). Tbr1 regulates differentiation of the preplate and layer 6. Neuron *29*, 353-366.

Hu, B.Y., Du, Z.W., and Zhang, S.C. (2009). Differentiation of human oligodendrocytes from pluripotent stem cells. Nat Protoc *4*, 1614-1622.

Jakovcevski, I., Filipovic, R., Mo, Z., Rakic, S., and Zecevic, N. (2009). Oligodendrocyte development and the onset of myelination in the human fetal brain. Front Neuroanat *3*, 5.

Jakovcevski, I., and Zecevic, N. (2005a). Olig transcription factors are expressed in oligodendrocyte and neuronal cells in human fetal CNS. J Neurosci *25*, 10064-10073.

Jakovcevski, I., and Zecevic, N. (2005b). Sequence of oligodendrocyte development in the human fetal telencephalon. Glia *49*, 480-491.

Jiang, P., Chen, C., Liu, X.B., Pleasure, D.E., Liu, Y., and Deng, W. (2016). Human iPSC-Derived Immature Astroglia Promote Oligodendrogenesis by Increasing TIMP-1 Secretion. Cell Rep.

Jiang, P., Chen, C., Wang, R., Chechneva, O.V., Chung, S.H., Rao, M.S., Pleasure, D.E., Liu, Y., Zhang, Q., and Deng, W. (2013). hESC-derived Olig2+ progenitors generate a subtype of astroglia with protective effects against ischaemic brain injury. Nat Commun *4*, 2196.

Kessaris, N., Fogarty, M., Iannarelli, P., Grist, M., Wegner, M., and Richardson, W.D. (2006). Competing waves of oligodendrocytes in the forebrain and postnatal elimination of an embryonic lineage. Nat Neurosci *9*, 173-179.

Klambt, C. (2009). Modes and regulation of glial migration in vertebrates and invertebrates. Nat Rev Neurosci *10*, 769-779.

Lancaster, M.A., Renner, M., Martin, C.A., Wenzel, D., Bicknell, L.S., Hurles, M.E., Homfray, T., Penninger, J.M., Jackson, A.P., and Knoblich, J.A. (2013). Cerebral organoids model human brain development and microcephaly. Nature *501*, 373-379.

Li, W., Sun, W., Zhang, Y., Wei, W., Ambasudhan, R., Xia, P., Talantova, M., Lin, T., Kim, J., Wang, X., *et al.* (2011). Rapid induction and long-term self-renewal of primitive neural precursors from human embryonic stem cells by small molecule inhibitors. Proc Natl Acad Sci U S A *108*, 8299-8304.

Ligon, K.L., Fancy, S.P., Franklin, R.J., and Rowitch, D.H. (2006). Olig gene function in CNS development and disease. Glia *54*, 1-10.

Liu, Y., Jiang, P., and Deng, W. (2011). OLIG gene targeting in human pluripotent stem cells for motor neuron and oligodendrocyte differentiation. Nat Protoc *6*, 640-655.

Livak, K.J., and Schmittgen, T.D. (2001). Analysis of relative gene expression data using real-time quantitative PCR and the 2(-Delta Delta C(T)) Method. Methods *25*, 402-408.

Loebrich, S., and Nedivi, E. (2009). The function of activity-regulated genes in the nervous system. Physiol Rev *89*, 1079-1103.

Lundgaard, I., Luzhynskaya, A., Stockley, J.H., Wang, Z., Evans, K.A., Swire, M., Volbracht, K., Gautier, H.O., Franklin, R.J., Charles, F.-C., *et al.* (2013). Neuregulin and BDNF induce a switch to NMDA receptor-dependent myelination by oligodendrocytes. PLoS Biol *11*, e1001743.

Madhavan, M., Nevin, Z.S., Shick, H.E., Garrison, E., Clarkson-Paredes, C., Karl, M., Clayton, B.L.L., Factor, D.C., Allan, K.C., Barbar, L., *et al.* (2018a). Induction of myelinating oligodendrocytes in human cortical spheroids. Nat Methods.

Madhavan, M., Nevin, Z.S., Shick, H.E., Garrison, E., Clarkson-Paredes, C., Karl, M., Clayton, B.L.L., Factor, D.C., Allan, K.C., Barbar, L., *et al.* (2018b). Induction of myelinating oligodendrocytes in human cortical spheroids. Nat Methods *15*, 700-706.

Mansour, A.A., Goncalves, J.T., Bloyd, C.W., Li, H., Fernandes, S., Quang, D., Johnston, S., Parylak, S.L., Jin, X., and Gage, F.H. (2018). An in vivo model of functional and vascularized human brain organoids. Nat Biotechnol *36*, 432-441.

Marchetto, M.C., Brennand, K.J., Boyer, L.F., and Gage, F.H. (2011). Induced pluripotent stem cells (iPSCs) and neurological disease modeling: progress and promises. Hum Mol Genet *20*, R109-115.

Mariani, J., Coppola, G., Zhang, P., Abyzov, A., Provini, L., Tomasini, L., Amenduni, M., Szekely, A., Palejev, D., Wilson, M., *et al.* (2015). FOXG1-Dependent Dysregulation of GABA/Glutamate Neuron Differentiation in Autism Spectrum Disorders. Cell *162*, 375-390.

Marton, R.M., Miura, Y., Sloan, S.A., Li, Q., Revah, O., Levy, R.J., Huguenard, J.R., and Pasca, S.P. (2019). Differentiation and maturation of oligodendrocytes in human three-dimensional neural cultures. Nat Neurosci *22*, 484-491.

Meijer, D.H., Kane, M.F., Mehta, S., Liu, H., Harrington, E., Taylor, C.M., Stiles, C.D., and Rowitch, D.H. (2012). Separated at birth? The functional and molecular divergence of OLIG1 and OLIG2. Nat Rev Neurosci *13*, 819-831.

Miller, D.J., Duka, T., Stimpson, C.D., Schapiro, S.J., Baze, W.B., McArthur, M.J., Fobbs, A.J., Sousa, A.M., Sestan, N., Wildman, D.E., *et al.* (2012). Prolonged myelination in human neocortical evolution. Proc Natl Acad Sci U S A *109*, 16480-16485.

Mitew, S., Gobius, I., Fenlon, L.R., McDougall, S.J., Hawkes, D., Xing, Y.L., Bujalka, H., Gundlach, A.L., Richards, L.J., Kilpatrick, T.J., *et al.* (2018). Pharmacogenetic stimulation of neuronal activity increases myelination in an axon-specific manner. Nat Commun *9*, 306.

Miyoshi, G., Butt, S.J., Takebayashi, H., and Fishell, G. (2007). Physiologically distinct temporal cohorts of cortical interneurons arise from telencephalic Olig2-expressing precursors. J Neurosci *27*, 7786-7798.

Monzel, A.S., Smits, L.M., Hemmer, K., Hachi, S., Moreno, E.L., van Wuellen, T., Jarazo, J., Walter, J., Bruggemann, I., Boussaad, I., *et al.* (2017). Derivation of Human Midbrain-Specific Organoids from Neuroepithelial Stem Cells. Stem Cell Reports *8*, 1144-1154.

Nagy, B., Hovhannisyan, A., Barzan, R., Chen, T.J., and Kukley, M. (2017). Different patterns of neuronal activity trigger distinct responses of oligodendrocyte precursor cells in the corpus callosum. PLoS Biol *15*, e2001993.

Nery, S., Wichterle, H., and Fishell, G. (2001). Sonic hedgehog contributes to oligodendrocyte specification in the mammalian forebrain. Development *128*, 527-540.

Nieto, M., Monuki, E.S., Tang, H., Imitola, J., Haubst, N., Khoury, S.J., Cunningham, J., Gotz, M., and Walsh, C.A. (2004). Expression of Cux-1 and Cux-2 in the subventricular zone and upper layers II-IV of the cerebral cortex. J Comp Neurol *479*, 168-180.

Nistor, G.I., Totoiu, M.O., Haque, N., Carpenter, M.K., and Keirstead, H.S. (2005). Human embryonic stem cells differentiate into oligodendrocytes in high purity and myelinate after spinal cord transplantation. Glia *49*, 385-396.

Ohara, P.T., Vit, J.P., Bhargava, A., Romero, M., Sundberg, C., Charles, A.C., and Jasmin, L. (2009). Gliopathic pain: when satellite glial cells go bad. Neuroscientist *15*, 450-463.

Ono, K., Takebayashi, H., Ikeda, K., Furusho, M., Nishizawa, T., Watanabe, K., and Ikenaka, K. (2008). Regional- and temporal-dependent changes in the differentiation of Olig2 progenitors in the forebrain, and the impact on astrocyte development in the dorsal pallium. Dev Biol *320*, 456-468.

Orentas, D.M., Hayes, J.E., Dyer, K.L., and Miller, R.H. (1999). Sonic hedgehog signaling is required during the appearance of spinal cord oligodendrocyte precursors. Development *126*, 2419-2429.

Pasca, A.M., Sloan, S.A., Clarke, L.E., Tian, Y., Makinson, C.D., Huber, N., Kim, C.H., Park, J.Y., O'Rourke, N.A., Nguyen, K.D., *et al.* (2015). Functional cortical neurons and astrocytes from human pluripotent stem cells in 3D culture. Nat Methods *12*, 671-678.

Pasca, S.P. (2018). The rise of three-dimensional human brain cultures. Nature *553*, 437-445.

Petryniak, M.A., Potter, G.B., Rowitch, D.H., and Rubenstein, J.L. (2007). Dlx1 and Dlx2 control neuronal versus oligodendroglial cell fate acquisition in the developing forebrain. Neuron *55*, 417-433.

Piao, J., Major, T., Auyeung, G., Policarpio, E., Menon, J., Droms, L., Gutin, P., Uryu, K., Tchieu, J., Soulet, D., *et al.* (2015). Human embryonic stem cell-derived oligodendrocyte progenitors remyelinate the brain and rescue behavioral deficits following radiation. Cell Stem Cell *16*, 198-210.

Pologruto, T.A., Sabatini, B.L., and Svoboda, K. (2003). ScanImage: flexible software for operating laser scanning microscopes. Biomed Eng Online *2*, 13.

Qian, X., Nguyen, H.N., Song, M.M., Hadiono, C., Ogden, S.C., Hammack, C., Yao, B., Hamersky, G.R., Jacob, F., Zhong, C., *et al.* (2016). Brain-Region-Specific Organoids Using Mini-bioreactors for Modeling ZIKV Exposure. Cell *165*, 1238-1254.

Rakic, S., and Zecevic, N. (2003). Early oligodendrocyte progenitor cells in the human fetal telencephalon. Glia *41*, 117-127.

Sessa, A., Mao, C.A., Colasante, G., Nini, A., Klein, W.H., and Broccoli, V. (2010). Tbr2-positive intermediate (basal) neuronal progenitors safeguard cerebral cortex expansion by controlling amplification of pallial glutamatergic neurons and attraction of subpallial GABAergic interneurons. Genes Dev *24*, 1816-1826.

Setoguchi, T., and Kondo, T. (2004). Nuclear export of OLIG2 in neural stem cells is essential for ciliary neurotrophic factor-induced astrocyte differentiation. J Cell Biol *166*, 963-968.

Stacpoole, S.R., Spitzer, S., Bilican, B., Compston, A., Karadottir, R., Chandran, S., and Franklin, R.J. (2013). High yields of oligodendrocyte lineage cells from human embryonic stem cells at physiological oxygen tensions for evaluation of translational biology. Stem Cell Reports *1*, 437-450.

Sun, L.O., Mulinyawe, S.B., Collins, H.Y., Ibrahim, A., Li, Q., Simon, D.J., Tessier-Lavigne, M., and Barres, B.A. (2018). Spatiotemporal Control of CNS Myelination by Oligodendrocyte Programmed Cell Death through the TFEB-PUMA Axis. Cell *175*, 1811-1826 e1821.

Suzuki, K., Bose, P., Leong-Quong, R.Y., Fujita, D.J., and Riabowol, K. (2010). REAP: A two minute cell fractionation method. BMC Res Notes *3*, 294.

Takebayashi, H., Yoshida, S., Sugimori, M., Kosako, H., Kominami, R., Nakafuku, M., and Nabeshima, Y. (2000). Dynamic expression of basic helix-loop-helix Olig family members: implication of Olig2 in neuron and oligodendrocyte differentiation and identification of a new member, Olig3. Mech Dev *99*, 143-148.

Tao, Y., and Zhang, S.C. (2016). Neural Subtype Specification from Human Pluripotent Stem Cells. Cell Stem Cell *19*, 573-586.

Tashiro, A., Goldberg, J., and Yuste, R. (2002). Calcium oscillations in neocortical astrocytes under epileptiform conditions. J Neurobiol *50*, 45-55.

Tekki-Kessaris, N., Woodruff, R., Hall, A.C., Gaffield, W., Kimura, S., Stiles, C.D., Rowitch, D.H., and Richardson, W.D. (2001). Hedgehog-dependent oligodendrocyte lineage specification in the telencephalon. Development *128*, 2545-2554.

Tosic, M., Rakic, S., Matthieu, J., and Zecevic, N. (2002). Identification of Golli and myelin basic proteins in human brain during early development. Glia *37*, 219-228.

Tripathi, R.B., Clarke, L.E., Burzomato, V., Kessaris, N., Anderson, P.N., Attwell, D., and Richardson, W.D. (2011). Dorsally and ventrally derived oligodendrocytes have similar electrical properties but myelinate preferred tracts. J Neurosci *31*, 6809-6819.

Vazin, T., Ball, K.A., Lu, H., Park, H., Ataeijannati, Y., Head-Gordon, T., Poo, M.M., and Schaffer, D.V. (2014). Efficient derivation of cortical glutamatergic neurons from human pluripotent stem cells: a model system to study neurotoxicity in Alzheimer's disease. Neurobiol Dis *62*, 62-72.

Voronova, A., Yuzwa, S.A., Wang, B.S., Zahr, S., Syal, C., Wang, J., Kaplan, D.R., and Miller, F.D. (2017). Migrating Interneurons Secrete Fractalkine to Promote Oligodendrocyte Formation in the Developing Mammalian Brain. Neuron *94*, 500-516 e509.

Wang, S., Bates, J., Li, X., Schanz, S., Chandler-Militello, D., Levine, C., Maherali, N., Studer, L., Hochedlinger, K., Windrem, M., *et al.* (2013). Human iPSC-derived oligodendrocyte progenitor cells can myelinate and rescue a mouse model of congenital hypomyelination. Cell Stem Cell *12*, 252-264.

Weidenheim, K.M., Kress, Y., Epshteyn, I., Rashbaum, W.K., and Lyman, W.D. (1992). Early myelination in the human fetal lumbosacral spinal cord: characterization by light and electron microscopy. Journal of neuropathology and experimental neurology *51*, 142-149.

Winkler, C.C., Yabut, O.R., Fregoso, S.P., Gomez, H.G., Dwyer, B.E., Pleasure, S.J., and Franco, S.J. (2018). The Dorsal Wave of Neocortical Oligodendrogenesis Begins Embryonically and Requires Multiple Sources of Sonic Hedgehog. J Neurosci.

Wu, S., Xu, R., Duan, B., and Jiang, P. (2017). Three-Dimensional Hyaluronic Acid Hydrogel-Based Models for In Vitro Human iPSC-Derived NPC Culture and Differentiation. J Mater Chem B *5*, 3870-3878.

Xiang, Y., Tanaka, Y., Patterson, B., Kang, Y.J., Govindaiah, G., Roselaar, N., Cakir, B., Kim, K.Y., Lombroso, A.P., Hwang, S.M., *et al.* (2017). Fusion of Regionally Specified hPSC-Derived Organoids Models Human Brain Development and Interneuron Migration. Cell Stem Cell *21*, 383-398 e387.

Xiao, J., Kilpatrick, T.J., and Murray, S.S. (2009). The role of neurotrophins in the regulation of myelin development. Neurosignals *17*, 265-276.

Xue, H., Wu, J., Li, S., Rao, M.S., and Liu, Y. (2016). Genetic Modification in Human Pluripotent Stem Cells by Homologous Recombination and CRISPR/Cas9 System. Methods Mol Biol *1307*, 173-190.

Xue, H., Wu, S., Papadeas, S.T., Spusta, S., Swistowska, A.M., MacArthur, C.C., Mattson, M.P., Maragakis, N.J., Capecchi, M.R., Rao, M.S., *et al.* (2009). A targeted neuroglial reporter line generated by homologous recombination in human embryonic stem cells. Stem Cells *27*, 1836-1846.

Zhao, J.W., Raha-Chowdhury, R., Fawcett, J.W., and Watts, C. (2009). Astrocytes and oligodendrocytes can be generated from NG2+ progenitors after acute brain injury: intracellular localization of oligodendrocyte transcription factor 2 is associated with their fate choice. Eur J Neurosci *29*, 1853-1869.

Zhong, S., Zhang, S., Fan, X., Wu, Q., Yan, L., Dong, J., Zhang, H., Li, L., Sun, L., Pan, N., *et al.* (2018). A single-cell RNA-seq survey of the developmental landscape of the human prefrontal cortex. Nature *555*, 524-528.

Figure legends:

Figure 1. Temporal expression of OLIG2 in hPSC-derived VFOs and DFOs.
(A) A schematic procedure for deriving brain region-specific forebrain organoids from OLIG2-GFP hPSCs by the treatment of a combination of sonic hedgehog (SHH) and purmorphamine (Pur) or cyclopamine (CycA) alone for VFOs and DFOs, respectively. The stages after week 3 are color-coded based on the expression of GFP.
(B) Representative bright-field and fluorescence images of embryoid bodies (EBs) at week 1, neural rosettes at week 2, primitive neural progenitor cells (pNPCs) at week 3, and VFOs and DFOs at week 5. pNPCs at week 3 were positive for PAX6 staining. Scale bars: 100 μm for bright-field images and 500 μm for fluorescence images.
(C) Representative images of the ventricular zone (VZ)-like structure formed by βIIIT$^+$ and SOX2$^+$ cells in DFOs at week 6. Scale bars, 50 μm.
(D and E) Representative images and quantification of Nestin-, FOXG1-, NKX2.1-, and PAX6-expressing cells in week 5 VFOs or DFOs (n = 4).
(F) qRT-PCR results showing the expression of *NKX2.2*, *DLX1*, *LHX6, EMX1,* and *TBR2* in week 5 VFOs and DFOs. The expression level was normalized to the GAPDH (n = 3). Student's *t*-test., **p < 0.05 and ***p < 0.001.
(G) Temporal expression of GFP fluorescence in VFOs and DFOs. Scale bar: 300 μm in the original images and 100 μm in the enlarged images.
(H) qRT-PCR results showing the expression of *OLIG2* at different time points in the DFOs. The expression level is normalized to GAPDH (n = 4). One-way ANOVA with Turkey's post hoc test. **p < 0.01.

Figure 2. Cellular localization of OLIG2 in VFOs and DFOs.
(A) Representative images showing OLIG2 expression in VFOs (left) and DFOs (right) at week 5. Scale bars, 100 μm and 50 μm in the original and enlarged images, respectively.
(B) Quantification of the percentage of GFP$^+$, OLIG2$^+$, and GFP$^+$/OLIG2$^+$ cells in the VFOs and DFOs at week 5 (n = 4).
(C) Quantification of the percentage of GFP$^+$ cells with nuclear or cytoplasmic OLIG2 expression among total GFP$^+$ cells (n = 3). Student's *t*-test., ***p < 0.001.
(D) Western blot showing the cellular localization of OLIG2 extracted from week 5 organoids. The experiments were repeated for three times. For each experiment, at least 10 VFOs or DFOs derived from OLIG2-GFP hESCs and hiPSCs were pooled for protein extraction and fractionation.
(E) Representative images of NKX2.1$^+$/GFP$^+$ cells in VFOs (top panels) and PAX6$^+$/GFP$^+$ cells in DFO (bottom panels). Scale bars, 50 μm and 10 μm in the original and enlarged images, respectively.
(F) Quantification of percentage of GFP$^+$/PAX6$^-$ cells and GFP$^+$/PAX6$^+$ cells in week 5 DFOs (n = 5).

Figure 3. Neuronal differentiation of OLIG2$^+$ cells in DFOs.
(A) Time-lapse images and representative traces of Ca^{2+} transients in DFOs. ROIs of active Fluo-4$^+$ cells were marked in red or green.
(B) Quantification of Ca^{2+} transients. Two distinct patterns of Ca^{2+} transients were identified: type 1 "glial cell-like pattern (green) and type 2 "neuron-like" pattern (red). Scale bars represent 50 s and 100% ΔF/F. Quantification for the number, peak value, and duration of the Ca^{2+} transients (n = 5 fields from 2 organoids) are shown.
(C and D) Representative images and quantification of the percentages of GFP$^+$/S100β^+ and GFP$^+$/βIIIT$^+$ cells among total GFP$^+$ cells (n = 3). Scale bars, 100 μm and 20 μm in the original and enlarged images, respectively.
(E and F) Representative images showing co-localization of GFP with DCX or TBR2 in week 7 DFOs. Scale bars, 100 μm and 50 μm in the original and enlarged images for DCX. Scale bars, 40 μm and 20 μm in the original and enlarged images for TBR2.

(G) Representative images showing co-localization of VGLUT1 and GFP. Scale bars, 20 μm. Arrows indicate VGLUT1 puncta along a GFP^+ process.
(H) Representative images showing co-localization of GLS, GFP, and βIIIT in week 7 DFOs. Arrows indicate a $GFP^+/\beta IIIT^+/GLS^+$ neuron in the top panels of enlarged images, and arrowheads indicate a GFP^+ cell that was GLS-negative in the bottom panels of enlarged images. Scale bars, 80 μm and 40 μm for top panels and bottom panels, respectively.

Figure 4. Oligodendrogenesis in VFOs and DFOs after neuronal maturation promoted by BrainPhys medium.
(A) A schematic diagram and representative images showing c-Fos expression in week 9 DFOs culture with neuronal differentiation (ND) medium (left) and BrainPhys medium (right). Scale bar, 100 μm.
(B) Quantification of the percentage of c-Fos^+ cells in the DFOs cultured under different conditions (n = 4). Student's *t*-test. *p < 0.05. Data are mean ± SEM.
(C) Representative images showing synapsin 1 and PSD-95 puncta in week 12 DFOs cultured in the BrainPhys medium. Scale bar, 20 μm.
(D) Representative images showing $TBR1^+$ and $CUX1^+$ cells in week 12 DFOs cultured in BrainPhys medium. Scale bar, 100 μm.
(E and F) Representative images and quantification showing the double-staining of EMX1 and GFP in week 10 DFO culture in BrainPhys medium (n = 4). Scale bars, 100 μm and 50 μm in the original and enlarged images, respectively.
(G) Representative images showing the expression of OPC marker $PDGFR\alpha^+$ in week 12 VFOs and DFOs. Arrows indicate the cells that are positive for PDGFRα and GFP. Scale, 100 μm.
(H) Quantification of the percentage of GFP^+ and $GFP^+/PDGFR\alpha^+$ cells in VFOs and DFOs (n = 4). Data are mean ± S.E.M. Student's *t*-test. *p < 0.05.
(I) Representative images showing that some $PDGFR\alpha^+$ OPCs express Ki67. Scale bars, 100 μm and 50 μm in the original and enlarged images, respectively.
(J) Representative images showing $TrkB^+/GFP^+$ cells are found in VFOs, but not in DFOs. Arrows indicate $TrkB^+/GFP^+$ cells. Arrowheads indicate $TrkB^-/GFP^+$ cells. Scale bars, 100 μm and 20 μm in the original and enlarged images, respectively.

Figure 5. Oligodendroglial maturation in DFOs, VFOs, and FFOs.
(A) A schematic procedure for fusing DFOs with VFOs and further culturing the FFOs in OL medium.
(B) Representative images showing the expression of GFP during the fusion process. FFOs are outlined with dotted lines at week 10 and 11. Scale bars, 200 μm, respectively.
(C) Representative images of MBP-expressing cells in VFOs, DFOs, and FFOs at week 12. Scale bar, 100 μm.
(D) Quantification of the percentage of MBP^+/GFP^+ cells in week 12 organoids (n = 4). Student's *t*-test. *p < 0.05. Data are mean ± S.E.M.
(E) Representative images showing a MBP^+ cell exhibiting complex processes in week 12 FFOs (left panel), and a MBP^+ cell exhibits tubular-shaped structure in week 15 FFOs (right panel). Scale bars, 20 μm and 10 μm in the original and enlarged images, respectively.
(F) Representative EM images of the myelin ultrastructure in FFOs at week 15. Scale bars, 1 μm and 100 nm.
(G) qRT-PCR results showing the expression of *SLC6A1*, *GAD1, SLC17A7*, *SLC17A6, SHANK3, HOMER1*, *GPHN, ARHGEF9*, *PDGFRα* and *MBP* in VFOs, DFOs, and FFOs. The expression level is normalized to GAPDH (n = 3). One-way ANOVA with Tukey post-hoc test., ***p < 0.05, **p < 0.01, and ***p < 0.001.

Figure 6. Interactions between dorsally- and ventrally-derived oligodendroglia in the FFOs.

(A) A schematic procedure for fusing the VFOs and DFOs that were respectively derived from isogenic OLIG2-GFP hiPSC reporter line and ND2.0 hiPSC line that do not have any reporter fluorescence.
(B and C) Representative images and quantification showing that ventrally-derived $OLIG2^+$ cells (GFP^+) are outnumbered by dorsally-derived $OLIG2^+$ cells (GFP-negative) at one week after fusion (week 10) to six weeks after fusion (week 15). Scale bar, 100 μm. Student's *t*-test., ***$p < 0.001$.
(D and E) Representative images and quantification showing the MBP^+ cells with a ventral (GFP^+) or dorsal (GFP-negative) origin. Scale bars, 50 μm. Student's *t*-test., ***$p < 0.001$.

Kim et al., Fig. 1

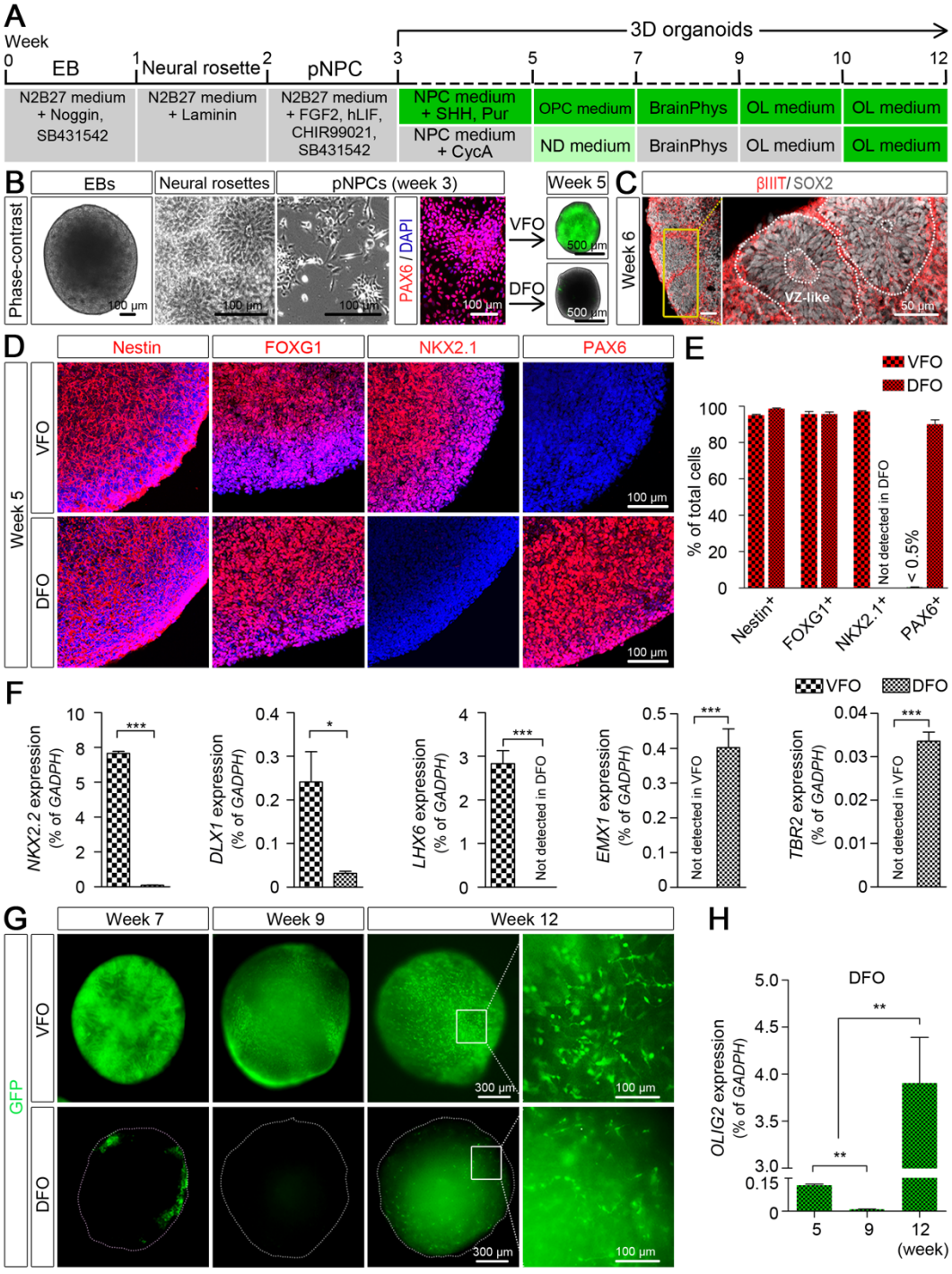

Kim et al., Fig. 2

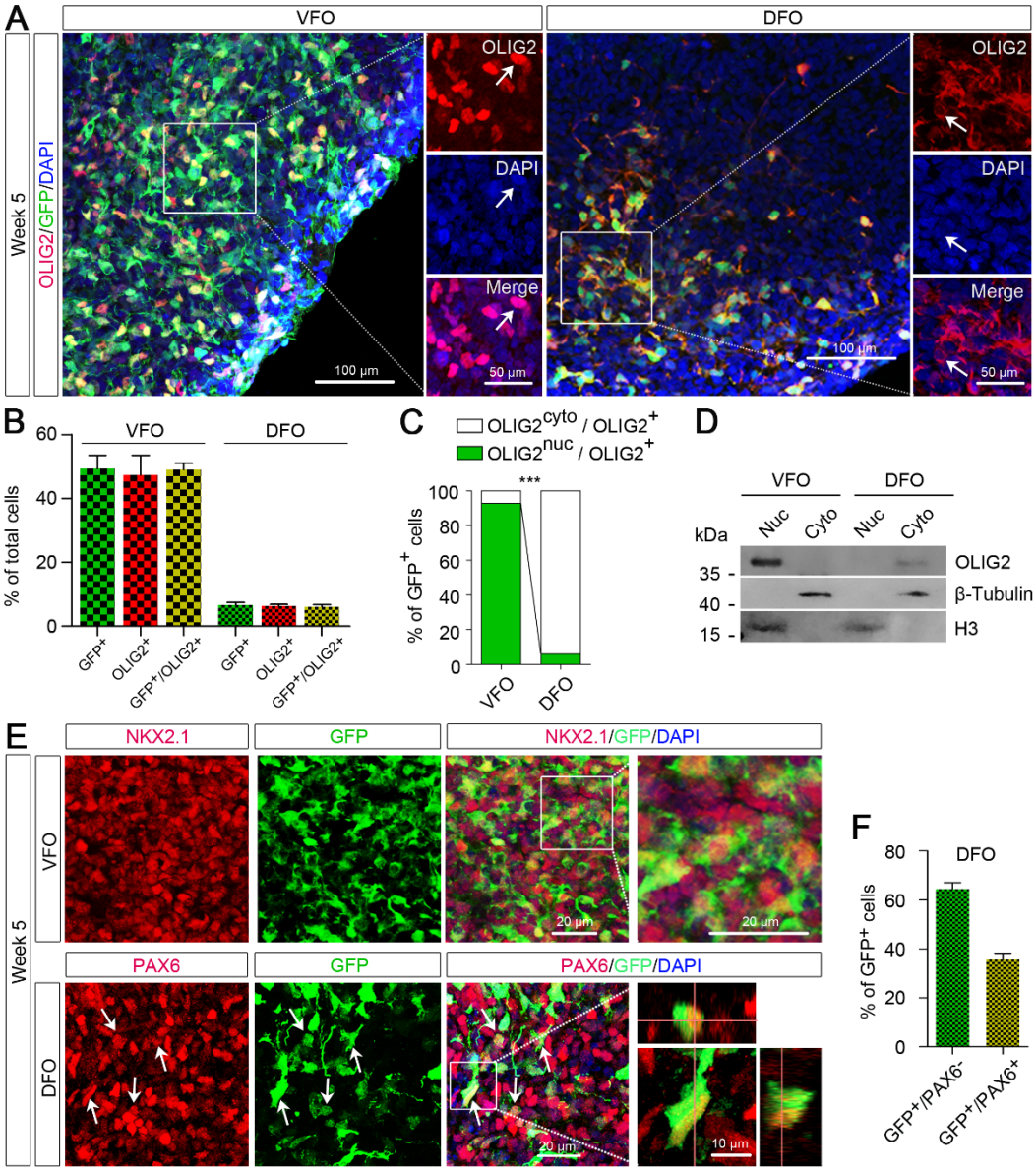

Kim et al., Fig. 3

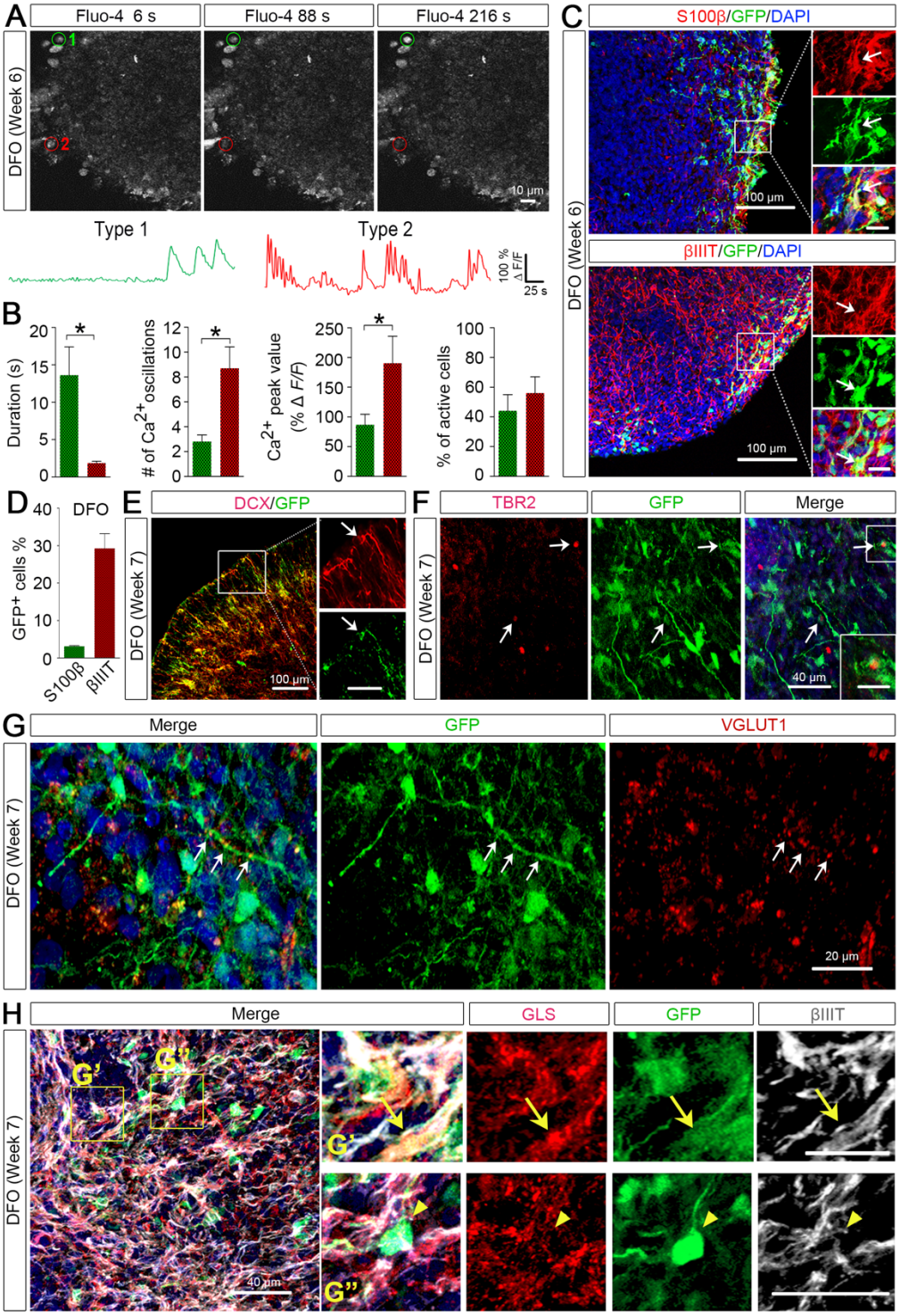

Kim et al., Fig. 4

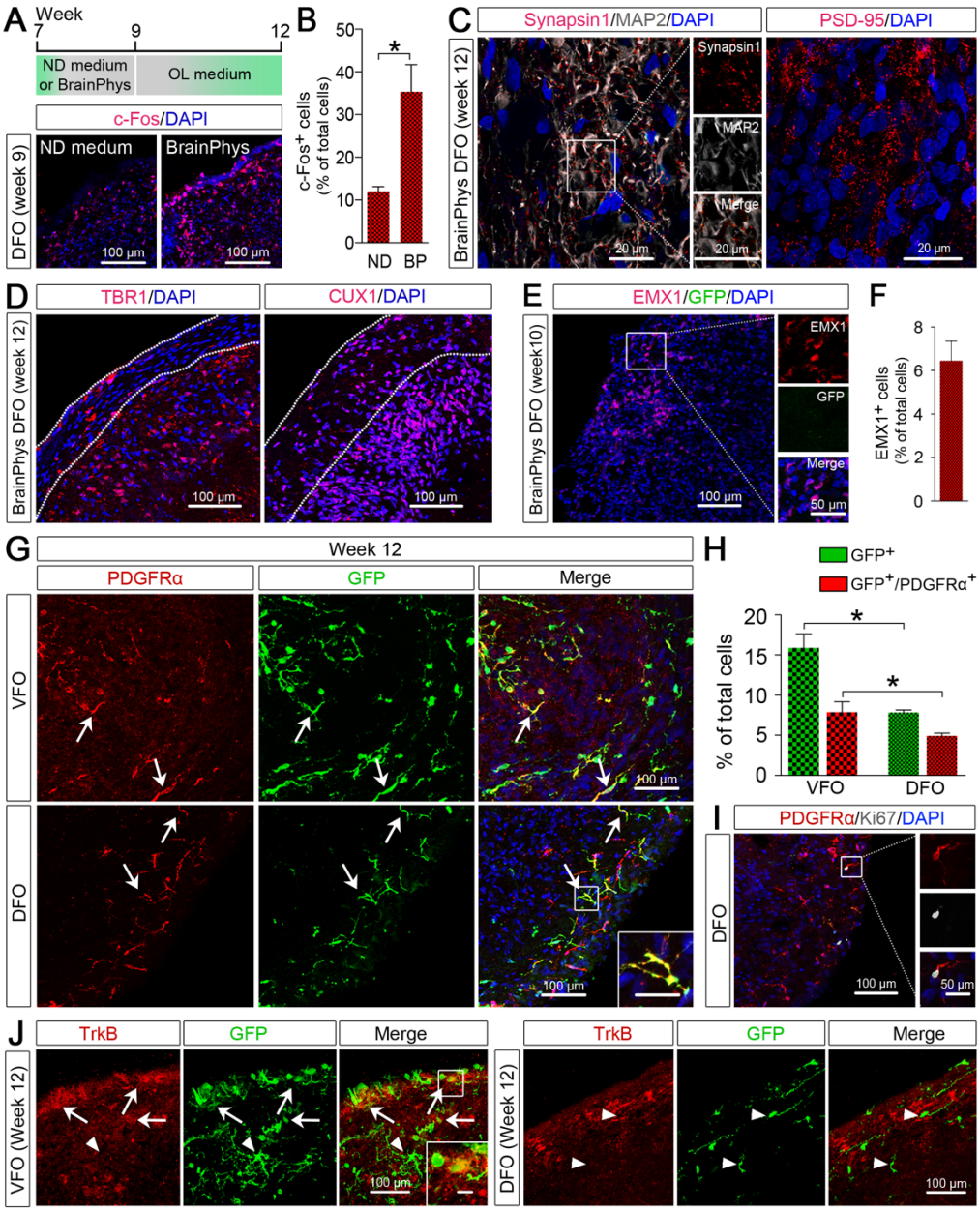

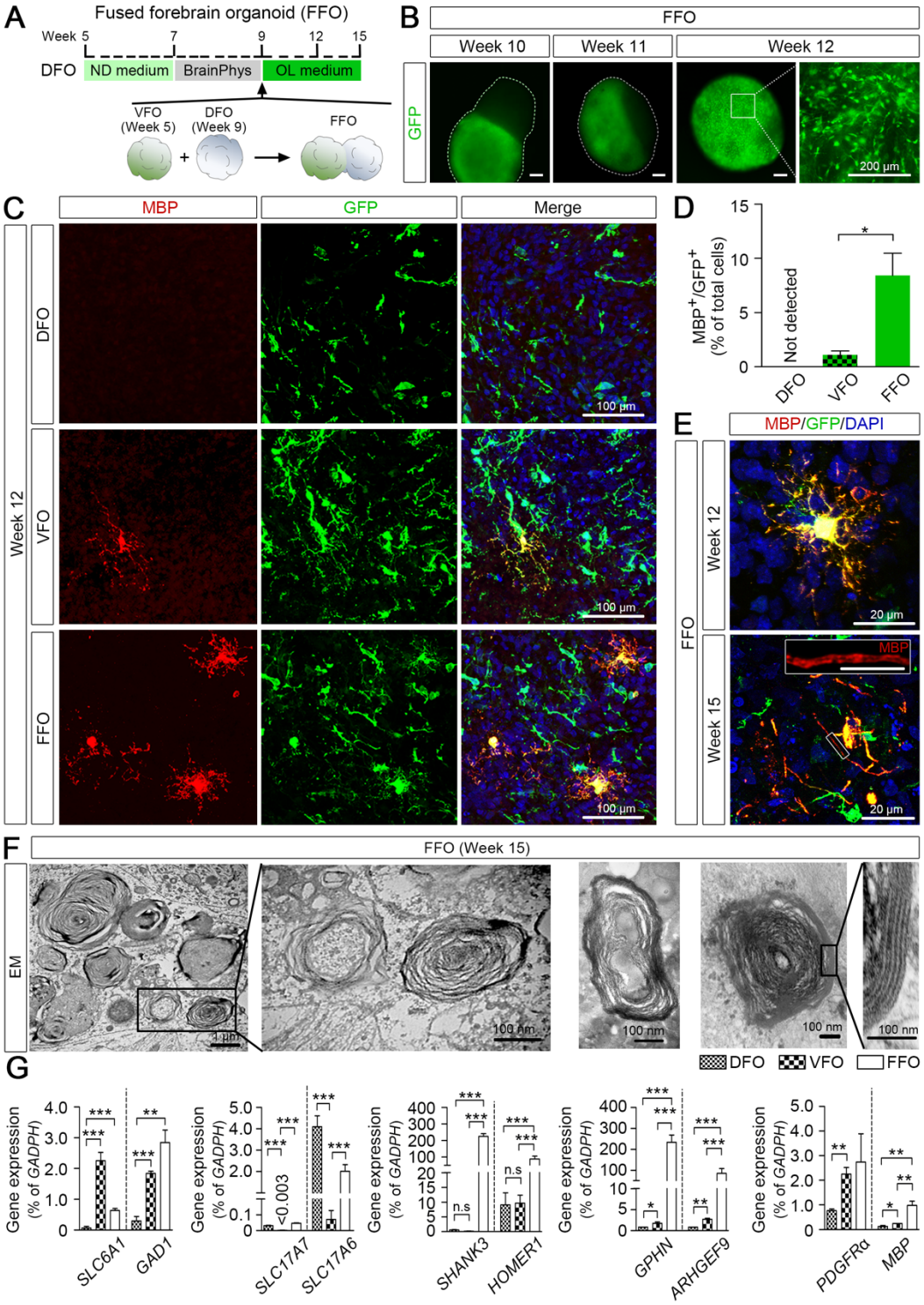

Kim et al., Fig. 6